American Journal of Engineering Research (AJER)
e-ISSN: 2320-0847 p-ISSN : 2320-0936
Volume-9, Issue-12, pp-157-166
www.ajer.org
Research Paper Open Access

Processing of 3D Radargrams Using Morphological Operations

T. Kishan Rao
Research Scholar, MG-NIRSA, University of Mysore, India
Former Executive Engineer, Irrigation Department
Government of Telangana, India

E. G. Rajan
Adjunct Professor, Department of Cybernetics
University of Petroleum and Energy Studies, Dehradun, India
Hon. Director MG-NIRSA, Hyderabad, India

Dr M Shankar Lingam
Research Associate, NIRDPR, Hyderabad

ABSTRACT
This paper provides a novel technique for processing 3D radargrams using mathematical morphological operations. The purpose of processing 3D radargrams is to extract useful information about the presence of subsurface elements and objects, be it oil, water, natural resources or man-made constructions. The term 'Morphological Filter' refers to once or repeated use of individual or combined operations of dilation and erosion with a single structuring element. Alternatively, the term 'Extended Morphological Filter' refers to once or repeated use of individual or combined operations of dilation and erosion with more than one structuring element. The technique proposed in this paper limits to the use of the operation of erosion on a 3D radargram for a finite number of times.

KEYWORDS*: Ground Penetrating Radar, Morphological Filtering, Subsurface Image Processing and Interpretation*

Date of Submission: 15-12-2020 Date of acceptance: 30-12-2020

I. INTRODUCTION

The aim of GPR based subsurface imaging is to obtain radargram images for subsurface truth evaluation, that is, to obtain a visual knowledge representation of the scene below the ground surface. Subsurface imaging deals with image data of very large size and thus a very large database has to be processed within given amount of time. This calls for development of fast and robust imaging algorithms with a high degree of reliability. Fig. 1 shows a 2D radargram of size 256×256 obtained using a GPR. This radargram is also called Vertical Seismic Profile (VSP). Fig. 1 also demonstrates how a set of radargram image slices obtained by B-scan, that is, moving a GPR antenna from a given position to another along a predetermined profile line.

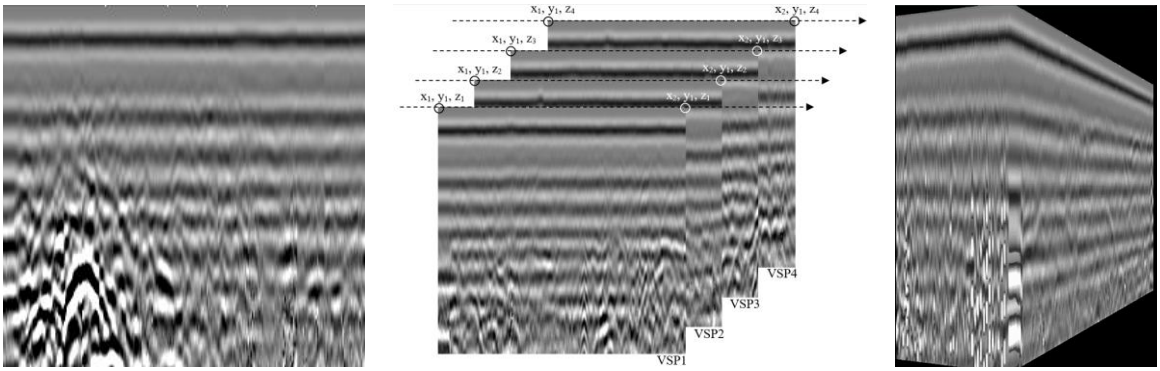

Fig. 1: Radargram slice, a set of slices and its 3D model of the entire 3D radargram slices

It is important that a 3D radargram data is interpreted for the very purpose for which it is obtained. In order to do this, a visual presentation of below the ground surface information is necessary. In other words, it is required to process the noise like radargram for a meaningful visual interpretation.

Real time 3D radargram slices obtained using a Ground Penetrating Radar (GPR)

Fig. 4 shows 81 slices named s1 to s81 obtained using a GPR in a site of specific defense interest in the USA. Each slice is called a Vertical Seismic Profile (VSP). All these 81 slices were obtained by moving a GPR in B-scan mode. Generally serpentine scanning is carried out to prospect a field of specific interest. Ground Penetration Radar (GPR) is used for excitation. Excitation is applied at appropriate locations, preferably at the centers of the sub divided regions. Fig. 2 shows excitation process as a serpentine scanning of a rectangular subsampled hypothetical field model. Fig. 3 shows a set of 81 slices of low resolution, each slice of which is of size 256×256 obtained after prospecting a real field of specific interest.

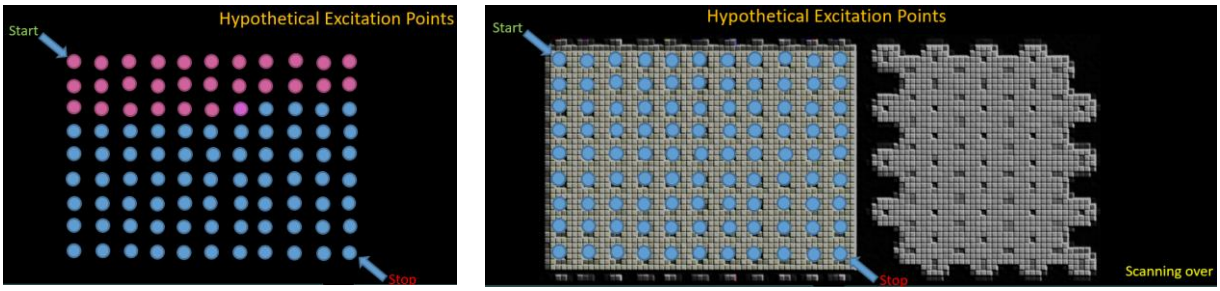

Fig. 2: Excitation process as a serpentine scanning of rectangular hypothetical field model

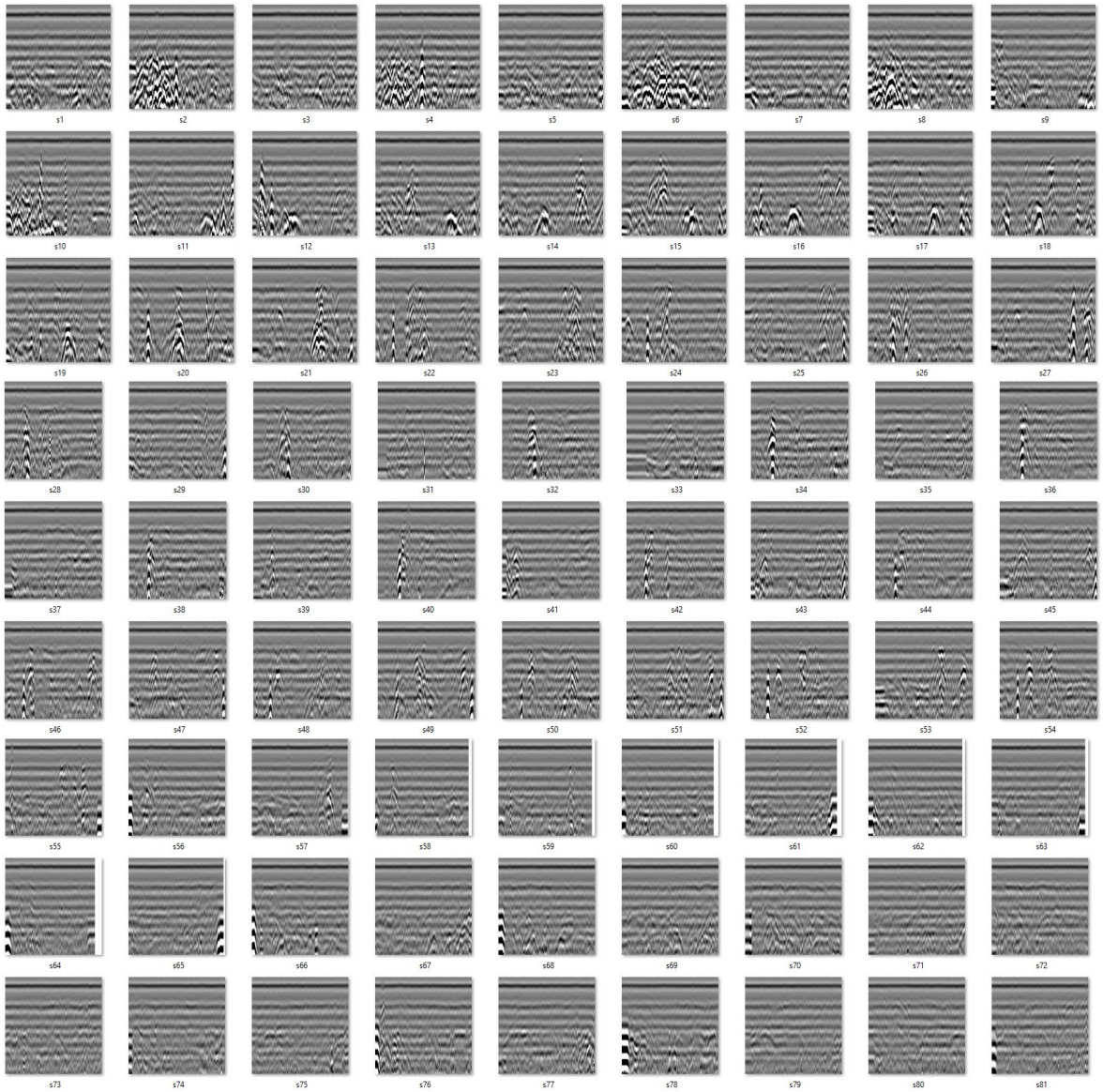

Fig. 3: Radargram slices of size 256×256×81

Ray casting technique – Basic principles

Volume ray casting is an image-ordering and volume rendering method. ***This computes a 2D image from the given 3D image***. A ray is cast for each voxel in a 3D image. The opacities observed in the path of a ray are accumulated till the ray exits the volume. The accumulated color/gray value is displayed as the 2D image pixel for every voxel in the 3D image.

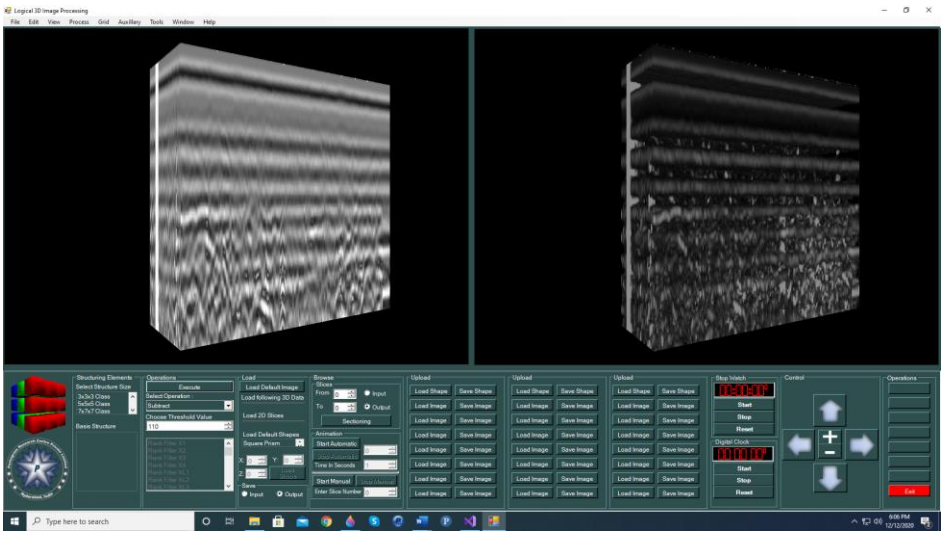

Fig. 4: Volume rendered 3D image and its intensity reduced version

Fig. 4 shows the volume rendered 3D radargram image and its intensity reduced version. Thus, given an ordered set of radargram slices, one can build a 3D radargram image and visualize it on a 2D monitor using ray casting method. The question that arises here is whether one would be able to process the 3D radargram image for whatever purpose it was built from 2D image slices. Traditionally, people use 2D image processing algorithms to process a 3D image, in which each slice is processed and the processed slices are integrated to build a 3D processed image. This is called 2.5D processing of 3D images. Alternatively, one can apply 3D image processing algorithms directly on the 3D radargram image, and this is called 3D processing of 3D images. Spatial domain and spectral domain approach in the 3D processing of 3D images are the two basic techniques practiced as on date. Three dimensional morphological operations play a significant role in spatial domain-based 3D processing. With the idea of evolving a practical method to extract morphological features of various subsurface elements a novel morphological filtering method to process a given 3D radargram is proposed in this paper.

II. MORPHOLOGICAL PROCESSING OF A 3D RADARGRAM

Let *f(p,q,r)* be a 3D gray scale image, where p is its height, q is its width and r is its depth. The domain D of a 3-D digital image is a subset of the 3-D grid Z^3: $f(p,q,r) \in D \subset Z^3$. One has to process 3D digital image morphologically with the help of a 3D structuring element. Fig. 5 shows various 3D neighborhood structures.

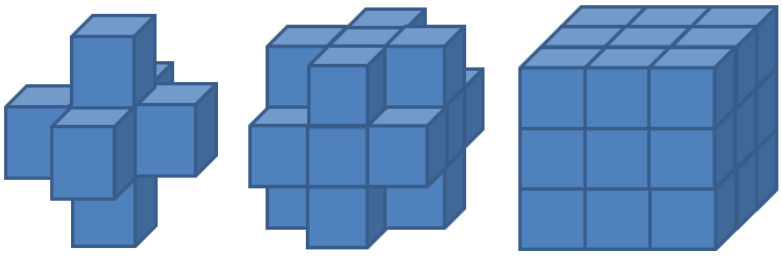

7-neighborhood 19-neighborhood 27-neighborhood

Fig. 5: Various 3D neighborhood structures

Appropriate structuring element is placed on the first 3D grid of voxels of the given 3D image. The output is set to the maximum/minimum value lying within the structuring element. The 3D structuring element is then moved across the 3D grid in that particular depth, until the entire 3D image in that depth has been processed. Then the structuring element is moved along the depth in the same way. The process is repeated until all the depths in 3D image have been processed.

3D Erosion of an input image *f(p,q,r)* by the 3D structuring element Z is defined as

$$Y = (f \ominus Z)(p,q,r) = \min_{z \in Z} f((p,q,r) + z) = \min_{g \in Z_x} G(p,q,r)$$

Example of 3D erosion is shown in the Fig. 6. Fig. 6 shows a bonsai 3D image and its eroded version. The bonsai tree shown in Fig. 6 is an MRI scanned data of a real bonsai tree. The 3D morphological erosion was applied on to this image and the eroded image is also shown in Fig. 6. One can clearly visualize the trunk and leaves of the tree by eroding the 3D image just once. This erosion operation has caused removal of one voxel 3D surface of every segmented component in the image. The 3D structuring element used for erosion is the 27-neighborhood shown in Fig. 5.

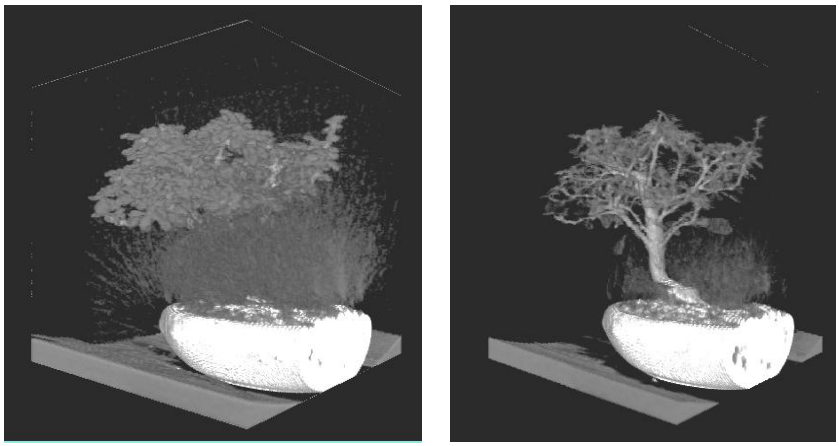

Original bonsai 3D image Image eroded by one voxel

Fig. 6: Bonsai 3-D image and its eroded version.

Erosion removes the outer cover of a 3D image. So, it is mandatory to know how many covers have to be removed to see the insides of a 3D image. This operation is similar to 'onion peeling' or 3D thinning. The advantage of carrying out this operation using morphological erosion is that one can have a choice of the nature of the outer cover that has to be removed and this is achieved using an appropriate structuring element.

Morphological erosion of 3D radargram

The 3D radargram image shown in Fig. 3 and Fig. 4 is morphologically eroded seven times continuously using the 27-neighborhood structuring element. Fig. 7, Fig. 8 and Fig. 9 respectively show the slices of 3D radargram eroded just once, twice and seven times. Fig. 10 shows the volume rendered 3D radargram image and its eroded versions. From Fig. 10, one observes that the seven times eroded radragram image shows some attributes related to some man-made structure. This was observed after eroding successively and it was not known a priori how many times one has to erode in order to get an image from which one can have a meaningful information.

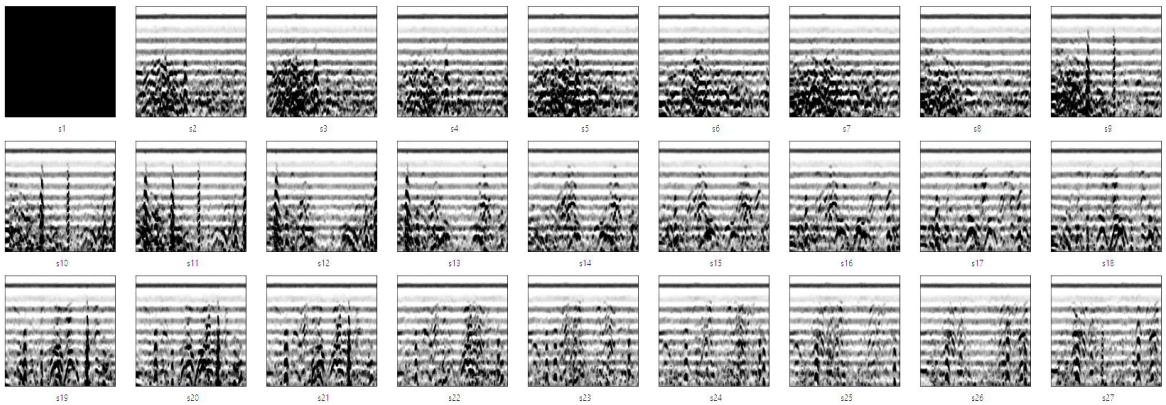

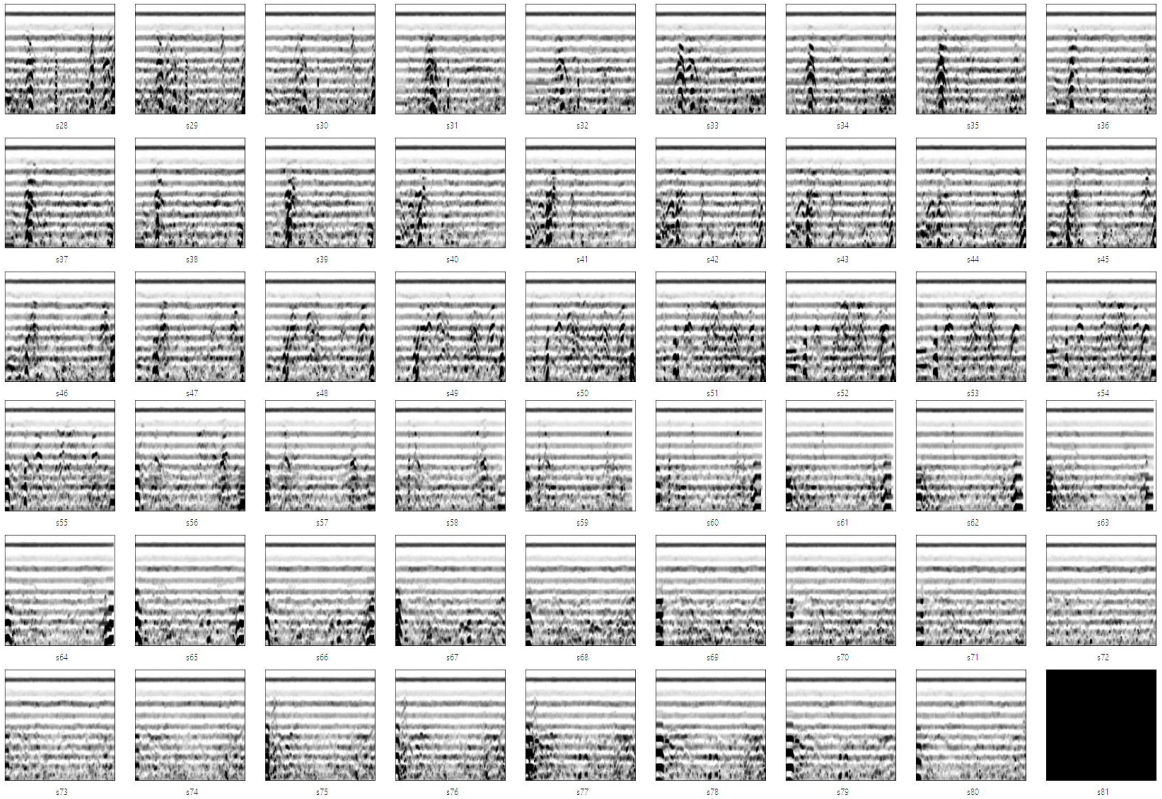

Fig. 7: Radargram of size 256×256×81 eroded once

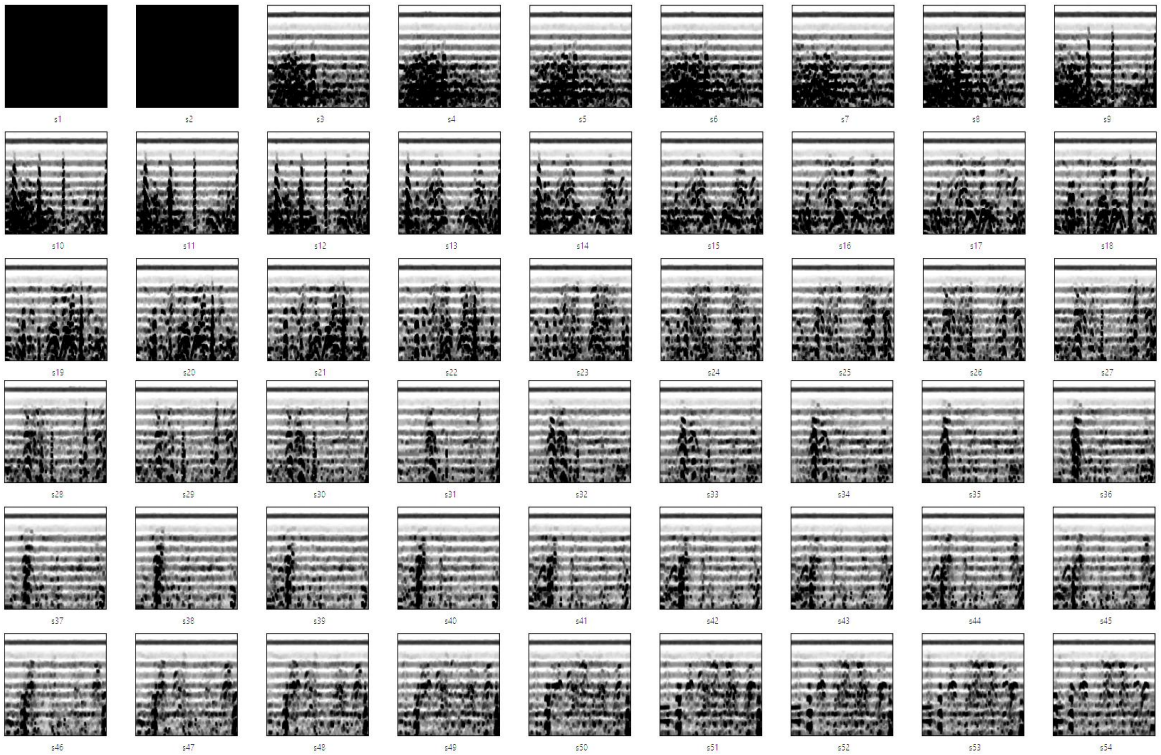

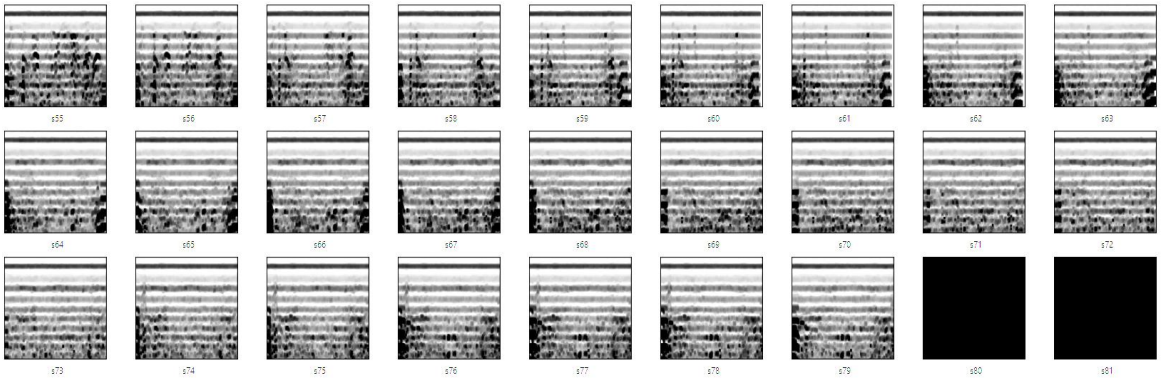

Fig. 8: Radargram of size 256×256×81 eroded twice

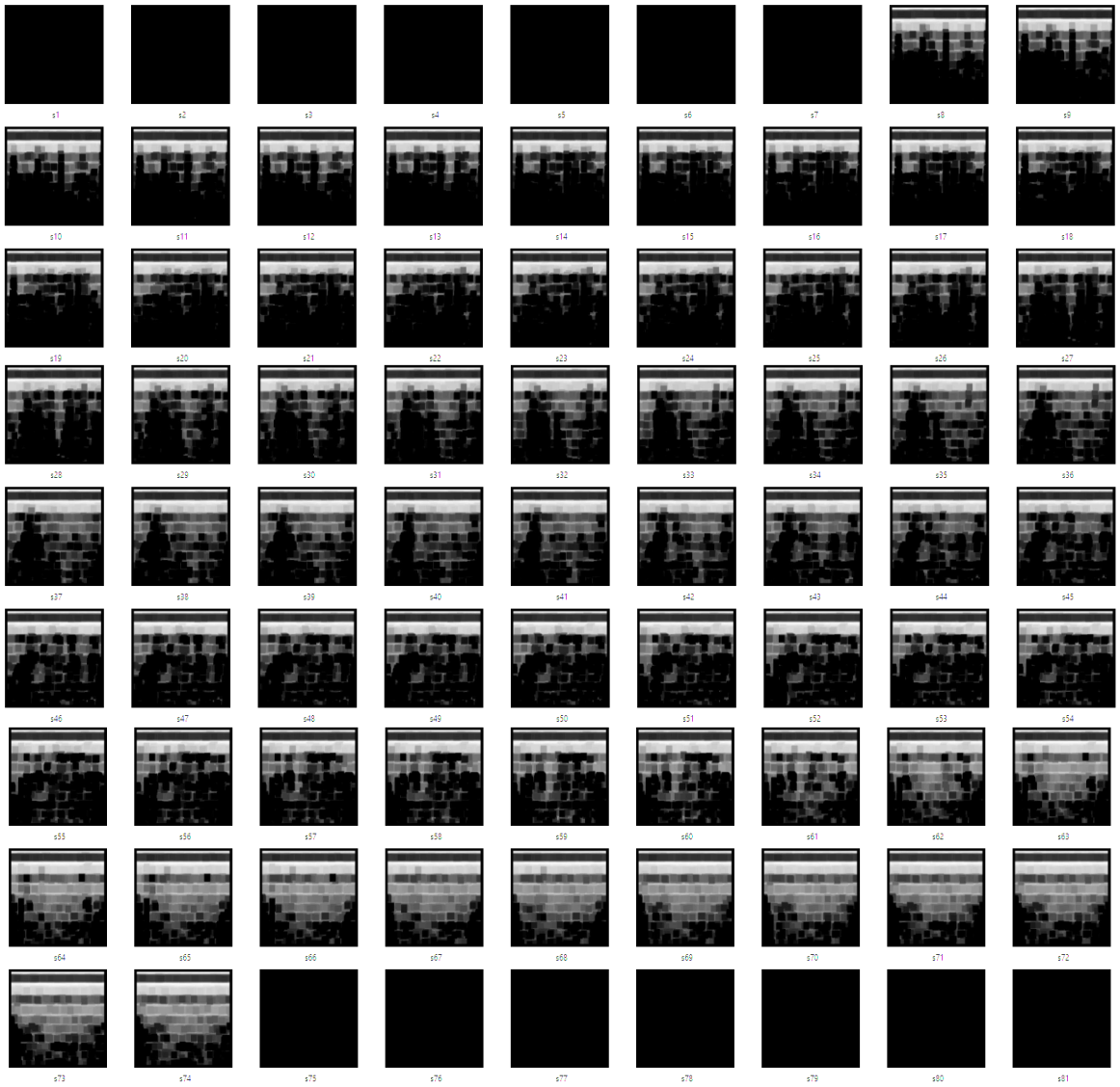

Fig. 9: Radargram of size 256×256×81 eroded seven times

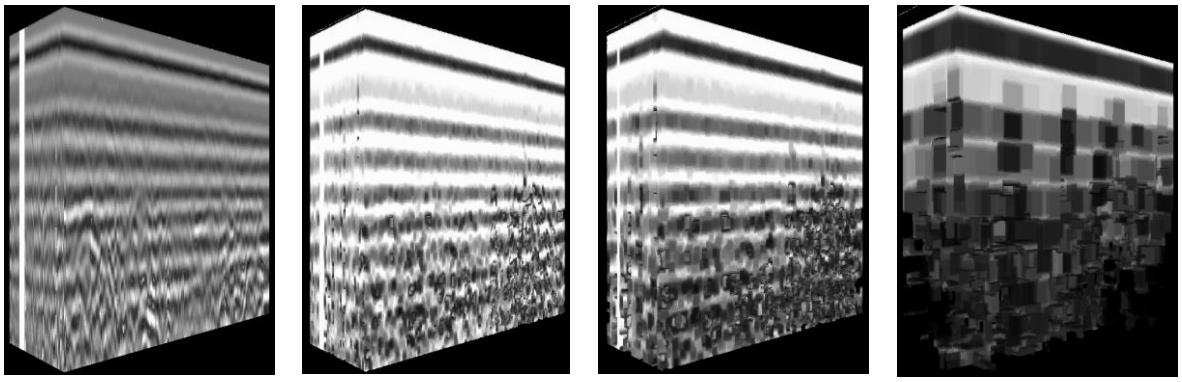

3D radargram image | Image eroded once | Image eroded twice | Image eroded seven times

Fig. 10: Volume rendered 3D radargram image and its eroded versions

The question that arises here is that how one can see the insides of the seven times eroded 3D radargram image, which shows the possibility of the presence of a man-made construction. A simple solution to this to detect the 3D edges of this image.

III. EDGE DETECTION OF MORPHOLOGICALLY FILTERED 3D RADARGRAM

3-D edge detection involves identification of edge voxels having maximum gradients. The given 3-D digital image is segmented by a threshold-based quantization scheme and at that moment boundaries of the quantized regions are extracted. The given 3-D digital image is plane-wise raster-scanned by the seven-neighborhood window which is shown in Fig. 5.

Algorithm for 3D edge detection

On every move, the 3×3×3 sub image enclosed by the seven-neighborhood window is examined to see whether the gray-distance D, which is the difference between the maximum and the minimum gray value corresponding to that sub image, is less than or equal to user specified threshold value T. If D is less than or equal to T, then the gray-value 0 is assigned to all the seven cells in the given image. For D greater than T, the original values contained in these cells are left undisturbed. This procedure is repeated until the entire image is scanned. The final result is that the edges of various 3D solid regions in the given image that appear to be uniform are retained and their left-over interior parts are erased thus giving us the edge of the original image. Fig. 11 shows a sample 3D image of a cell structure and its edge detected version.

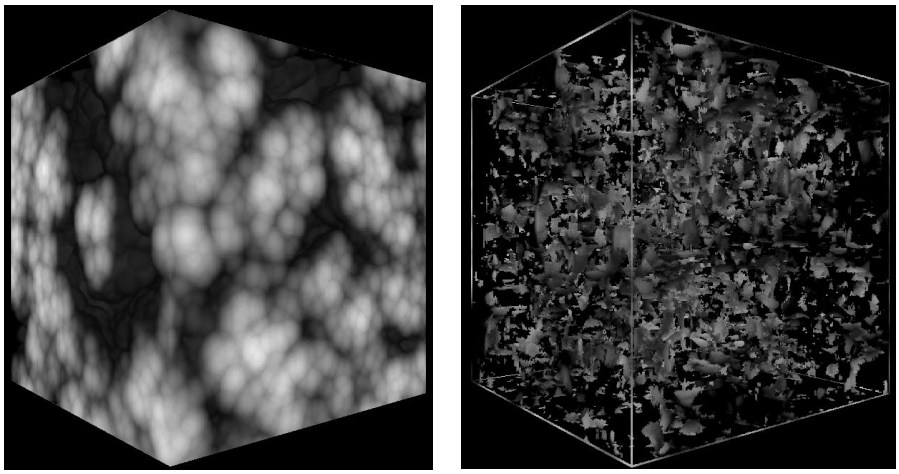

Sample 3D image of a cell structure | Edge detcted version of the 3D image

Fig. 11: Sample 3D image and its edge detected version

Fig. 12 shows 81 slices of 3D edge detected version of 7-times eroded 3D radargram of size 256×256×81.

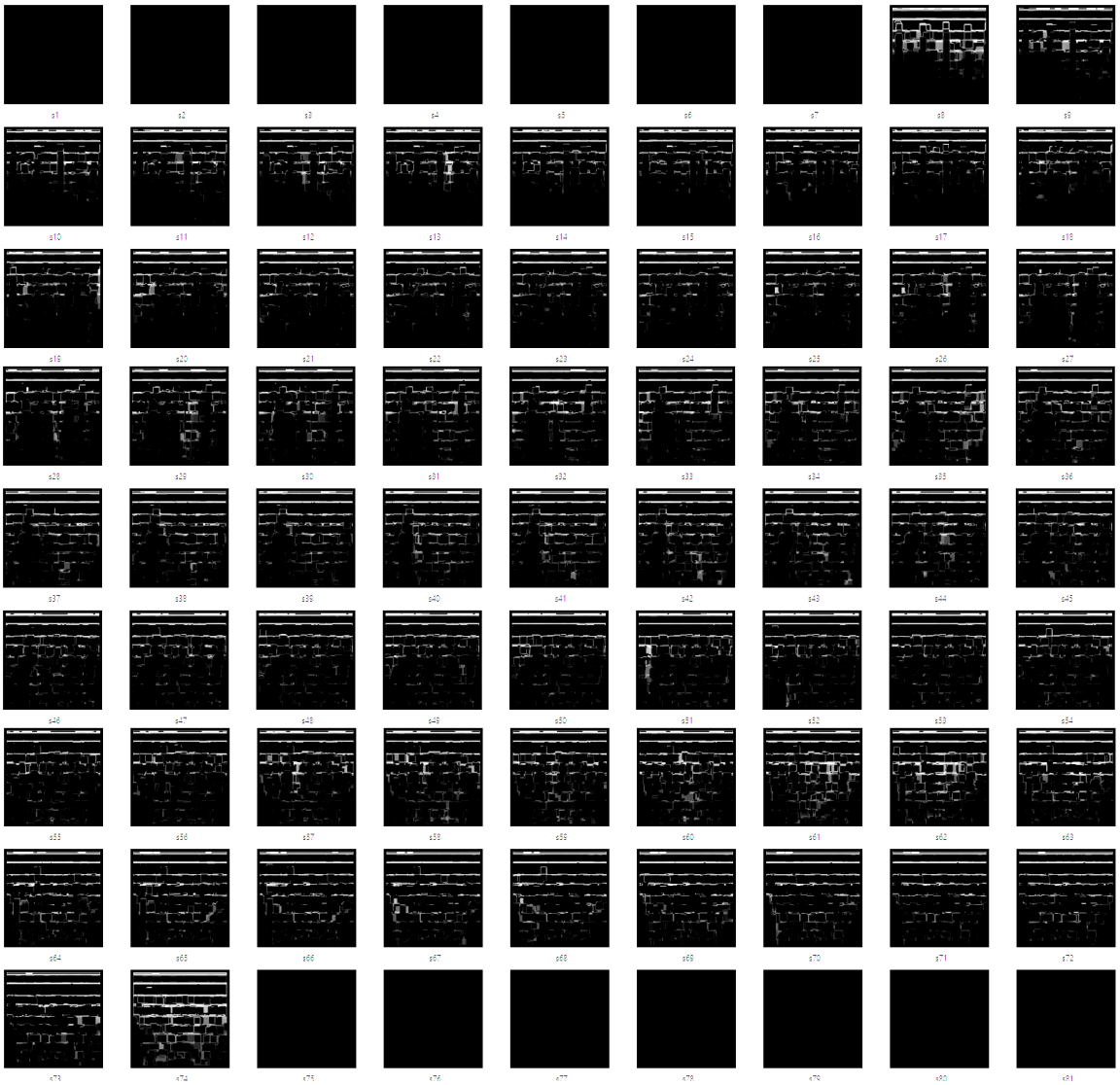

Fig. 12: Slices of 3D edge detected version of 7-times eroded 3D radargram of size 256×256×81

Fig. 13 shows the original 3D radargram image and the front and rear views of the image obtained using morphological filtering and edge detection.

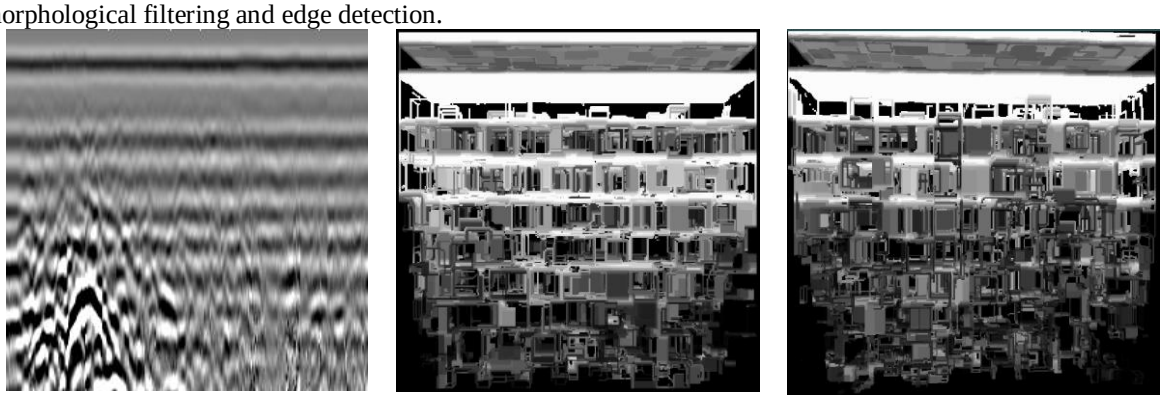

3D radargram image Front View Rear View

Fig. 13: Front and rear views of the processed 3D radargram image

Fig. 14 shows different side views of the processed 3D radargram image.

Observations

1. 3D edge detection yields an image that exposes the interiors of a solid model image.
2. With reference to Fig. 13 and Fig. 14, it is reasonable to conclude that the given 3D radargram was obtained by moving a GPR in B-scan trace.

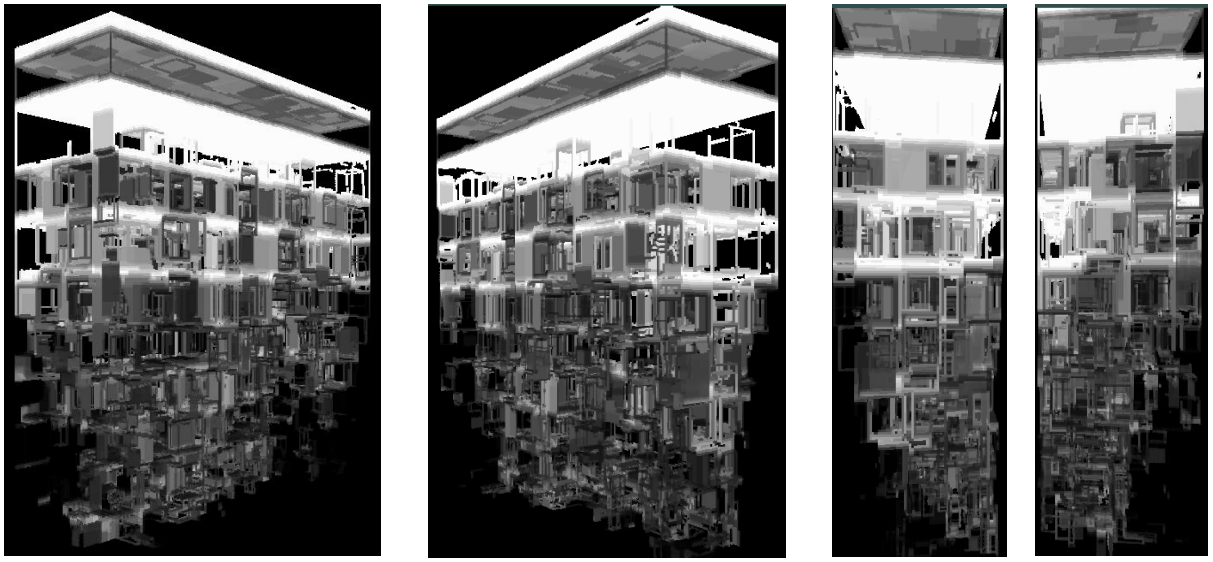

Left Anterior Oblique (LAO) View | Right Anterior Oblique (RAO) View | Left View | Right View

Fig. 14: Different side views of the processed 3D radargram image

IV. CONCLUSIONS

Morphological erosion is carried out to extract hidden information from a 3D radargram. In addition, 3D edge detection is done on the eroded image to extract its inner details. The number of times the erosion should be carried out is unknown a priori because that depends on the type of the site prospected by GPR.

ACKNOWLEDGEMENT

The authors put on records the support extended by MG-NIRSA, Hyderabad, Pentagram Research Centre Pvt Ltd., Hyderabad, University of Petroleum and Energy Studies, Dehradun and Avatar MedVision US LLC, NC, USA. Thanks are due to Dr. Shankar, MG-NIRSA for coordinating with University of Mysore while the first author was carrying out PhD.

Advisory Committee Members and Co-authors

1. Dr. Manish Prateek, Dean, School of Computer Science, UPES, Dehradun, India
2. Dr. Amit Agarwal, Director, APJ Abdul Kalam, Institute of Technology, Dehradun, India
3. Dr. Michael Patrick Coyle, Chief Executive Officer, Avatar MedVision US LLC, NC, USA
4. Sathya Govindarajan, Director, Pentagram Research Centre Private Limited, Hyderabad, India
5. Prashanthi Govindarajan, Director, Pentagram Research Centre Private Limited, Hyderabad, India
6. Yashaswi Vemuganti, Consultant, Avatar MedVision US LLC, NC, USA
7. Dr. Jean Claude Perez, IBM European Research Center on Artificial Intelligence, France
8. Dr. Hindupur Rajasimha, Chief Engineer, Indian Space Research Organization and IDBI (Retd.)

REFERENCES

[1]. Jean Serra; Cube, cube-octahedron or rhomb-dodecahedron as bases for 3-D shape descriptions, Advances in visual form analysis, World Scientific 1997, 502-519.
[2]. Wuthrich, C.A. and Stucki, P.; An algorithm comparison between square- and hexagonal based grids; Graphical Models and Image Processing, 53(4), 324–339,1991.
[3]. Reinhard Klette and Azriel Rosenfeld; Digital Geometry: Geometric methods for picture analysis; Elsevier, 2004.
[4]. B. Nagy; Geometry of Neighborhood sequences in hexagonal grid; Discrete Geometry of computer imagery; LNCS-4245, Springer.
[5]. Tristan Roussillon, Laure Tougne, and Isabelle Sivignon; What Does Digital Straightness tell about Digital Convexity?;
[6]. Edward Angel, "Interactive Computer Graphics- a top down approach with OpenGL", Second Edition, Addison Wesley, 2000.
[7]. S.W. Zucker, R.A. Hummel, "A Three-Dimensional Edge Operator", IEEE Trans. On PAMI, Vol. 3, May 1981.
[8]. Jürgen, H., Manner, R., Knittel, G., and Strasser, W. (1995). Three Architectures for Volume Rendering. International Journal of the Eurographics Association, 14, 111-122
[9]. Dachille, F. (1997). Volume Visualization Algorithms and Architectures. Research Proficiency Examination, SUNY at Stony Brook

[10]. Günther, T., Poliwoda, C., Reinhart, C., Hesser, J., and Manner, J. (1994). VIRIM: A Massively Parallel Processor for Real-Time Volume Visualization in Medicine. Proceedings of the 9th Eurographics Hardware Workshop, 103-108
[11]. Boer, M.De, Gröpl, A., Hesser, J., and Manner, R. (1996). Latency-and Hazard-free Volume Memory Architecture for Direct Volume Rendering. Eurographics Workshop on Graphics Hardware, 109-119
[12]. Swan, J.E. (1997). Object Order Rendering of Discrete Objects. PhD. Thesis, Department of Computer and Information Science, The Ohio State University
[13]. Yagel, R. (1996). Classification and Survey of Algorithms for Volume Viewing. SIGGRAPH tutorial notes (course 34)
[14]. Law, A. (1996). Exploiting Coherency in Parallel Algorithms for Volume Rendering. PhD. Thesis, Department of Computer and Information Science, The Ohio State University
[15]. Ray, H., Pfister, H., Silver, D., and Cook, T.A. (1999). Ray Casting Architectures for Volume Visualization. IEEE Transactions on Visualization and Computer Graphics, 5(3), 210-233
[16]. Yagel, R. (1996). Towards Real Time Volume Rendering. Proceedings of GRAPHICON' 96, 230-241
[17]. Kaufman, A.E. (1994). Voxels as a Computational Representation of Geometry. in The Computational Representation of Geometry SIGGRAPH '94 Course Notes
[18]. Lacroute, P., and Levoy, M. (1994). Fast Volume Rendering Using a Shear-Warp Factorization of the Viewing Transform. Computer Graphics Proceedings Annual Conference Series ACM SIGGRAPH, 451-458.
[19]. Sutherland, I.E., Sproull, R.F., and Schumaker, R.A. (1974) A Characterization of Ten Hidden Surface Algorithms. ACM Computing Surveys, 6(1), 1-55
[20]. Roberts, J.C. (1993). An Overview of Rendering from Volume Data including Surface and Volume Rendering. Technical Report 13-93*, University of Kent, Computing Laboratory, Canterbury, UK.
[21]. Frieder, G., Gordon, D., and Reynolds, R.A. (1985). Back-to-Front Display of Voxel-Based Objects. IEEE Computer Graphics and Applications, 5(1), 52-60
[22]. Westover, A.L. (1991). Splatting: A Parallel Feed-Forward Volume Rendering Algorithm. Ph.D. Dissertation, Department of Computer Science, The University of North Carolina at Chapel Hill
[23]. Zwicker, M., Pfister., H., Baar, J.B. and Gross M. (2001). Surface Splatting. In Computer Graphics SIGGRAPH 2001 Proceedings, 371-378
[24]. Nulkar, M., and Mueller, K. (2001). Splatting With Shadows. International Workshop on Volume Graphics 2001,35-50
[25]. J. Krüger and R. Westermann, Acceleration Techniques for GPU-based Volume Rendering, Proceedings of the 14th IEEE Visualization 2003 (VIS'03), 38-43.
[26]. Markus Hadwiger, Joe M. Kniss, Christ of Rezk-salama, Daniel Weiskopf, and Klaus Engel. Real time Volume Graphics. A. K. Peters, Ltd., USA, 2006.
[27]. Goodman, D., Nishimura, Y., Hongo, H and Noriaki N., 2006. Correcting for topography and the tilt of the GPR antenna, Archaeological Prospection, 13: 157-161.
[28]. Goodman, D., Y. Nishimura, and J. D. Rogers, 1995. GPR time slices in archaeological prospection: *Archaeological Prospection*, 2:85-89.
[29]. Goodman, D., 1994. Ground-penetrating radar simulation in engineering and archaeology: *GEOPHYSICS*, 59:224-232.

T. Kishan Rao, et. al. "Processing of 3D Radargrams Using Morphological Operations."*American Journal of Engineering Research (AJER)*, vol. 9(12), 2020, pp. 157-166.